PCCP

Accepted Manuscript

ROYAL SOCIETY OF CHEMISTRY

www.rsc.org/pccp

Recombination kinetics in silicon solar cell under low-concentration: Electro-analytical characterization of space-charge and quasi-neutral regions

Pankaj Yadav[1], Brijesh Tripathi[1, 2], Kavita Pandey[1], Manoj Kumar[2,*]

[1] School of Solar Energy, Pandit Deendayal Petroleum University, Gandhinagar – 382007 (India)

[2]School of Technology, Pandit Deendayal Petroleum University, Gandhinagar – 382007 (India)

*Corresponding Author: Ph: +91 79 2327 5428, Fax: +91 79 2327 5030,

Email: manoj.kumar@sse.pdpu.ac.in

TABLE OF CONTENTS ENTRY

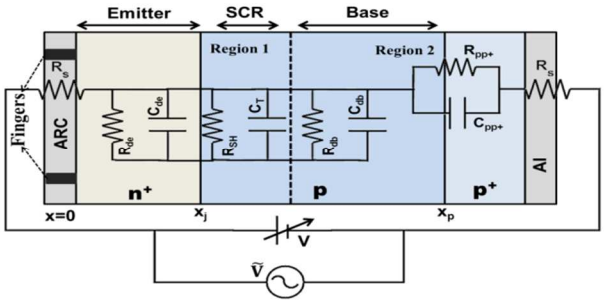

- Electro-analytical measurements to demonstrate the characteristic features of charge recombination in space-charge region and quasi-neutral region

ABSTRACT

Present work reports a detailed electro-analytical framework to study commercially available mono-crystalline silicon solar cells under varying illumination conditions to explore their application in upcoming field of low-concentration photovoltaics (LCPV). Effect of low concentration illumination (>1-12 suns) on performance indicating parameters, i.e., short-circuit current, open-circuit voltage, fill factor, efficiency and ideality factors were investigated using D.C. characterization. The same framework supports A.C. characterization to explore diffusion capacitance, transition capacitance, diffusion resistance and recombination kinetics under varying illumination scenario. Recent developments in impedance spectroscopy technique have broadened its horizon for various studies to address unexplored material and performance aspects of mono-crystalline Si solar cell under non-equilibrium conditions. The obtained D.C. and A.C. experimental results are coupled with theoretical treatment to demonstrate the characteristic features of charge recombination in space-charge region and quasi-neutral region.

KEYWORDS: Mono-crystalline silicon solar cell, low-concentration photovoltaics, quasi-neutral region, impedance spectroscopy

1. INTRODUCTION

Among the various existing PV materials, silicon (Si) is one of the most widely used semiconductors for the fabrication of solar cell. About 80% to 90% of PV modules manufactured worldwide are silicon wafer-based solar cell [1]. The cost of electricity generated from solar cell is quite high as compared to the conventional sources of energy i.e. hydroelectric, nuclear, thermal power etc. Further cost reduction of silicon solar cell is possible by using c-Si wafers [2], c-Si thin film [3], Si in the form of ribbon [4, 5] and concentrator Si solar cell [6, 7]. Low

concentration photovoltaic (LCPV) technology has proven to be an effective means for reducing the cost of photovoltaic electricity since early 1990's**.** In the last decade, the price of silicon based solar module is reduced by a factor of 1/5 making it more relevant to develop low concentration photovoltaic system using these cells for further energy market penetration. Si solar cell based LCPV systems with a concentration ratio below ~10 suns present two major advantages: (1) LCPV systems can use conventional high performance silicon solar cells (fabricated for 1 sun application [8]), (2) LCPV systems are less demanding in terms of tracking accuracy as compared to high concentration systems [9]. In recent years, significant advancement in the field of low concentration has been made by achieving peak efficiency of 15% at 14 suns using commercially available mono-crystalline single junction solar cells [10]. Castro et al estimated a cost of \$ 0.5/W_p for Si based concentration photovoltaic system [11] using back contact solar cell under 100 suns. Li et al have reported the performance of solar cell array based on trough concentrating photovoltaic/ thermal system [12].

Recently various research groups have shown modeling, design and construction of LCPV systems based on Si solar cell [3, 13-15] and few companies have invested in this technology for commercialization [10, 16-19]. It is well known that the existing Si-based PV technology warranty 25-30 years of use, in order to get a substantial share in PV industry the low concentration technology must provide similar warranty. For LCPV systems, an extensive study for system's reliability should be confirmed before issuing any such claim. Studies based on DC characterization of Si solar cell under low concentration in laboratory and real time analysis have been carried out in detail by various researchers [4-12]. In our previous articles, we have reported real time analysis of LCPV system and its dynamic behavior [1, 8, 20-22]. However, the major disadvantages of DC techniques used for solar cell characterization are: (1) it does not

particularly help for probing the AC parameters that are necessary for designing the dynamic load of such devices [23] and (2) the transient response of charge carriers is difficult to estimate, which is very important for understanding device behavior with respect to time.

In the present study, a combined DC and AC techniques have been used for the characterization of Si solar cell. AC impedance spectroscopy (IS) technique is used to examine the effective recombination lifetime by studying the recombination kinetics via resistance and capacitance measurements. Impedance spectroscopy is a small perturbation method that resolves the capacitance and resistance of electronic devices under test at steady state. Close to zero bias voltage, the operation of efficient solar cell is usually determined by charge separation and efficient collection. On the other hand, at the maximum power point close to V_{OC}, recombination kinetics (i.e. the effective recombination lifetime) plays a major role [24]. Only few reports exist in literature for probing the DC and AC characteristics of mono crystalline Si based solar cell [23-28], and to the best of our knowledge no report exists to explore the DC and AC parameters of mono-crystalline Si solar cell for low concentration applications. The present work focuses on number of performance indicating parameters i.e. include diffusion capacitance, resistance, ideality factor and minority carrier lifetime of Si solar cell that dominates the electrical response under various non-equilibrium conditions. The obtained experimental results are coupled with theoretical treatment to provide a framework for addressing unexplored material and performance aspects of Si solar cell under low concentration.

2. THEORETICAL CONSIDERATIONS

When a solar PV module is exposed to solar radiation, it shows non-linear current voltage characteristics. The non-linearity arises due to the loss of photo-generated carriers. The mechanism for photo-generated carrier loss has been accounted by many researchers [1, 3, 26].

These loss mechanisms include: (1) thermalization loss: photo-generated carriers move from initial excited state to the respective band edges, (2) spatial relaxation: the photo-generated carriers are swept along the band edges to the contacts, (3) radiative recombination of electron hole pair, (4) Shockley-Read-Hall, Auger and surface recombination (5) series and shunt resistances. All the discussed loss mechanism associated with photo generated carriers are described in terms of single or double diode model where the rectifying behavior and recombination losses of a solar cell are represented by diode 1 and diode 2 respectively. In this article, an effective diode model of a mono-crystalline silicon solar cell has been adopted [23, 25].

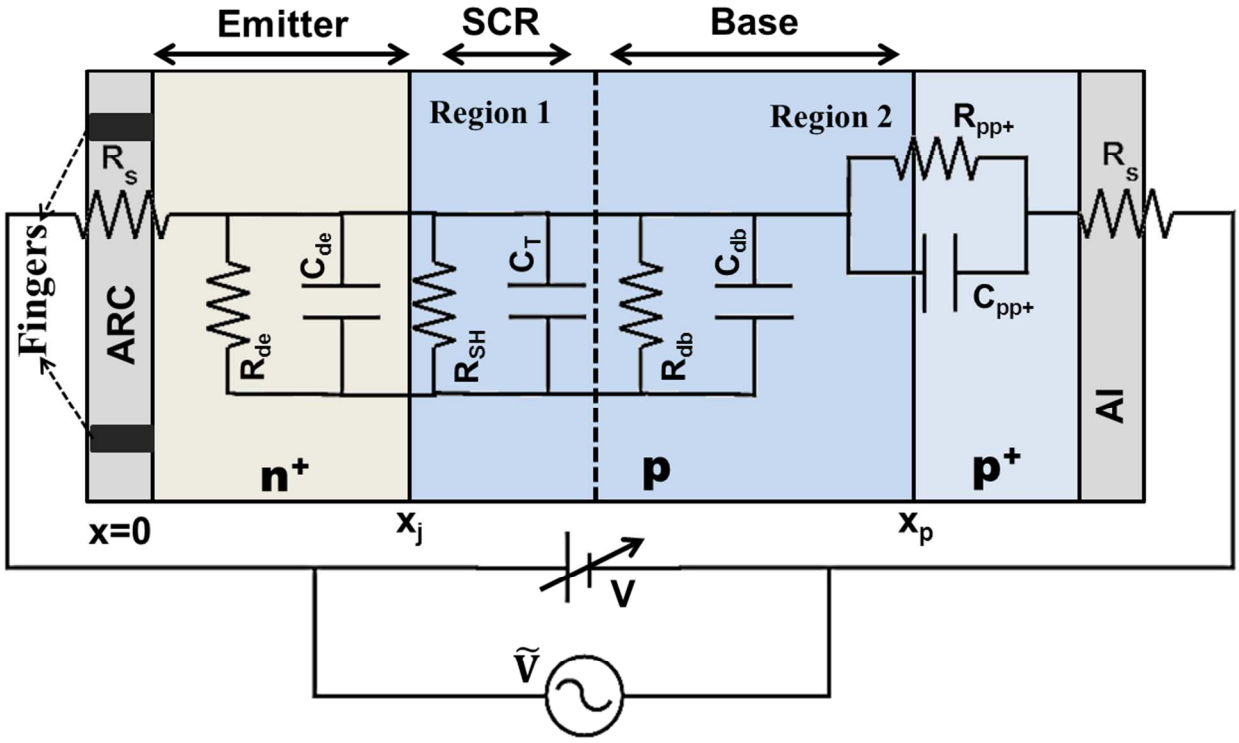

Fig. 1 Schematic of mono-crystalline Si solar cell with performance contributing elements from different regions

Fig. 1 schematically shows the basic layout of silicon solar cell with various regions offering different capacitive and resistive components during its operation. The terminal equation for current-voltage characteristics of the solar cell is given by [29, 30, 31]:

$$I = I_{PH} - I_d - \left(V + I\mathrm{R_S} - V_{pp^+}\right)/\mathrm{R_{SH}} \qquad (1)$$

The detailed explanation of various physical processes with respect to Fig. 1 is given in the supporting information. The diode current accounting for carrier recombination in n^+-p junction is governed by effective diode ideality factor (m) under forward bias and can be expressed in terms of voltage V_j:

$$\mathrm{I_d} = \mathrm{I_0}\left[\exp\left(\frac{|e|\mathrm{V_j}}{\mathrm{mk_BT}}\right) - 1\right] \qquad (2)$$

where, I_0 is the effective reverse saturation current of the diode which is a combination of contributions from space charge recombination (SCR) and quasi neutral recombination (QNR). The contributions from both the region are included by splitting I_0 in two parts: I_{01} and I_{02} for QNR and SCR respectively. Reverse current, I_{01} arises when band-to-band recombination takes place in QNR, while I_{02} arises due to impurity/trap-level recombination occurring in SCR. Under the higher bias condition, the recombination is high in QNR, so $I_0 \approx I_{01}$, with an ideality factor of $m \approx 1$. Whereas, under the low bias condition, the recombination is high in SCR, so $I_0 \approx I_{02}$, with an ideality factor of $m \approx 2$. For the single diode model of Si solar cell, the effective value of m is generally taken between 1 and 2, where the lower and upper bounds of m are expected at moderate and strong forward and reverse bias voltages respectively [23].

The aforementioned D.C. model alone is insufficient to analyze the different kinetics (diffusion, recombination and transportation of charge carrier) of the silicon solar cell under non equilibrium condition. Under these circumstances, electrochemical impedance spectroscopy (EIS) has been rigorously employed in explaining the charge transfer resistance, capacitance,

diffusion and charge recombination kinetics at n^+-p junction. The proposed A.C. equivalent circuit elements that allow the extraction of all relevant information about recombination kinetics of n^+-p junction solar cell is incorporated in Fig. 1. A direct current (D.C.) voltage '*V*' combined with small amplitude, time dependent perturbation voltage, $\tilde{V}$ is applied across the Si solar cell. R_S, R_{de}, R_{SH} and R_{db} represent the series resistance, emitter resistance, shunt resistance and the resistance offered by base respectively. The dependence of R_d on ideality factor (m) and junction diode current is given by Eq. (3) [23]:

$$R_d = \frac{mk_BT}{|e|exp\left(\frac{|e|V_j}{mk_BT}\right)}\left[\frac{1}{I_{0b}} + \frac{1}{I_{0e}}\right] \quad (3)$$

where V_j represents the junction voltage and I_{0e} and I_{0b} represent the current at emitter and base respectively. R_d is also known as recombination resistance (R_{rec}), which contains information about recombination flux. The total D.C. resistance (R_{dc}) of solar cell is defined by the reciprocal of negative derivative of current with respect to voltage, i.e. $-\left(dI/dV\right)^{-1}$. By taking the derivative of the current voltage terminal equation (Eq. (1)) the expression for R_{dc} is obtained as [25-28]:

$$R_{dc} = \frac{\left(R_d + R_s + R_{pp+}\right)}{\left[1 + I\left(\frac{\partial R_s}{\partial V}\right) + R_d\left(\frac{dI_{pp+}}{dV}\right)\right]} \quad (4)$$

At higher forward bias voltage, charge recombination in QNR is more dominating than SCR region. The net impedance (Z) of the equivalent circuit shown in Fig. 1 is a series combination of the impedances, Z_j and Z_{pp+} of the n^+-p and the p-p^+ junctions, respectively. The high frequency part of spectra contains information about the transport and series resistance elements as well as dielectric contributions, which is not treated in this paper. The low frequency arc contributes to recombination in the solar cell and capacitance, resistance and lifetime values [23, 24]. In order

to improve the performance and reliability of mono-crystalline Si solar cell under low concentration, the charge carrier dynamics and material aspects must be considered.

3. EXPERIMENTAL SECTION

3.1. Material aspects of mono-crystalline Si solar cell

The commercially available mono-crystalline Si solar cells procured from Nease Asia Pvt. Ltd. (India) is used in the present study. The procured solar cell is fabricated using p-type mono-crystalline silicon wafer as a starting material (acts as a base layer) in which gaseous $POCl_3$ is diffused for emitter fabrication. The silicon nitride layer (~ 80 nm) at the front surface of silicon solar cell works as an anti-reflecting coating and surface passivation layer. The use of silicon nitride layer improves the bulk minority carrier lifetime and diffusion lengths. The p-p^+ junction which act as a back surface field is formed by diffusing Aluminum in p-type base material. The aluminum (Al) at the back side results in Al gettering in which the metallic impurities from the bulk is either removed or dissolved, which enhances the carrier lifetime.

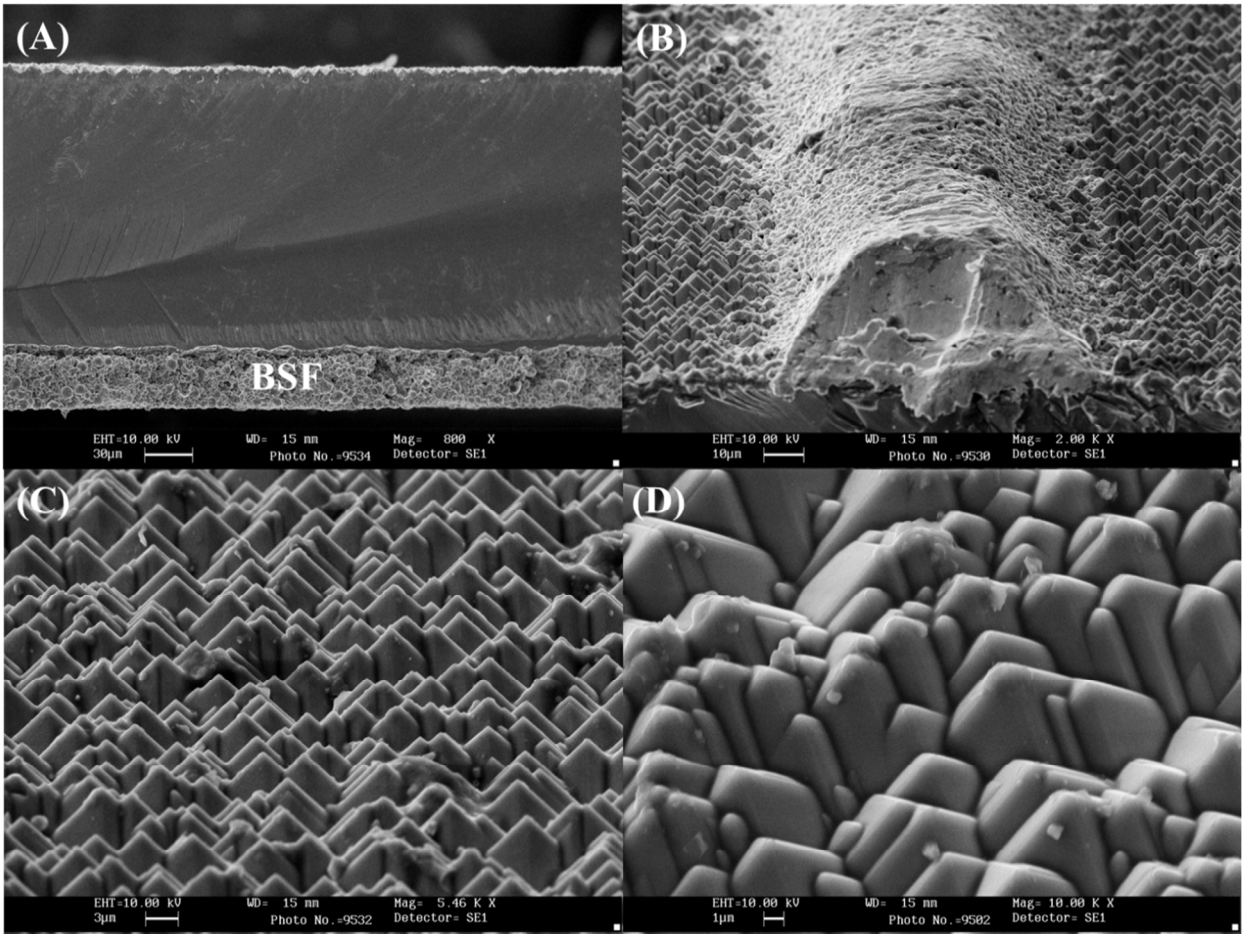

Fig. 2 SEM images of: (A) Cross-Sectional view of mono-crystalline Si solar cell; (B) enlarged view of a current carrying finger; (C) topography of mono-crystalline Si solar cell; (D) higher magnification image of topography showing pyramid structure

Fig. 2A shows the cross sectional view of mono-crystalline silicon solar cell with a thickness of ~ 215 µm having approx. 25 µm back surface layer of aluminum. Screen printing technology is used for front and back contact metallization. Fig. 2B shows the topography of silicon solar cell with a current carrying finger made from Ag based pastes. Fig. 2C shows the anisotropically etched surface of mono-crystalline silicon solar cell. The difference in the atomic density in

<100> and <111> direction leads to the formation of pyramids at the surface. Fig. 2D shows the high magnification image of the pyramids formed at solar cell surface in <100> direction.

The photovoltaic characteristic parameters short-circuit current (I_{SC}), open-circuit voltage (V_{OC}), fill factor (FF), and power conversion efficiency (η) of the solar cell under 1 sun illumination (AM1.5, 1000 W/m^2) are 11 mA, 509 mV, 62.1% and 12.9% respectively. The solar cell material parameters described here are used to explore the recombination kinetics by using impedance spectroscopy technique.

3.2. Device characterization

The solar cell I-V characterization was done by using solar simulator (Photoemission Tec SS80AAA with 1.5AM-G filter) and Source measuring unit (U2722A, Agilent). The temperature of the solar cell was measured by the digital thermometer (Mini Temp, Raytek) with an accuracy of ±2°C and Fresnel lens has been used for concentrating solar radiation. During measurements silicon solar cell was mounted over the heat sink to maintain constant temperature. The electron micrographs were collected using a Leo-s 440i Scanning Electron Microscope with an operating voltage range of 1−10 kV under ultrahigh vacuum conditions. A three electrode potentiostat (CHI 660D) equipped with a frequency analyzer was used for impedance spectroscopy (IS) measurements. The working electrode was connected to the positive terminal of Si solar cell (i.e. on back side) whereas counter electrode and reference electrode were sorted and connected to the negative front terminal of Si solar cell. A variable D.C. voltage source is used to apply a potential difference from -0.5 to 1.0 V across P-N junction with a scan rate of 5 mVs^{-1}. The inductive effects of connecting leads from Si solar cell to potentiostat have been taken care of during the experiments. IS data were collected in the form of Nyquist impedance spectra. During

IS measurements an A.C. perturbation of 5 mV root-mean-square voltage is applied in the frequency range 1 Hz to 0.1 MHz.

4. RESULT AND DISCUSSION

4.1. Diffusion controlled kinetic parameters

The impedance spectroscopy (IS) is used here to understand the diffusion controlled transport kinetics of commercially available Si solar cells having power conversion efficiency within the range of 12–16.8%. From these measurements, the influence of light concentration (> 1 sun) on charge carrier recombination process and on quasi-Fermi levels (which influence upper limit of achievable V_{OC}) have been explored by applying a forward bias voltage $V_F \simeq V_{OC}$.

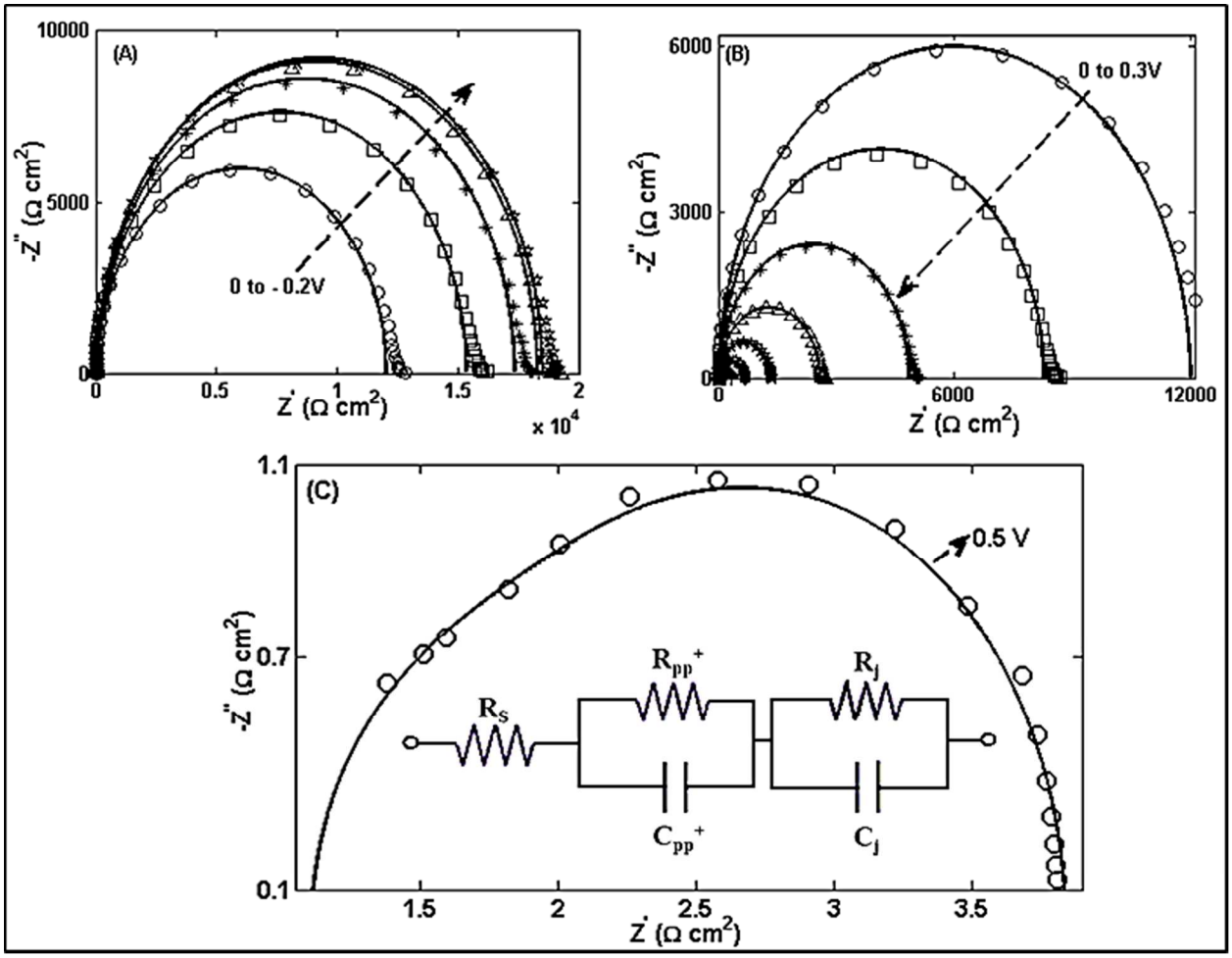

Fig. 3 Nyquist spectra for mono-crystalline Si solar cell (A) the plots were collected at decreasing voltages in the following order: V = 0, -0.05, -0.1, -0.15, -0.2 with arrow indicating the successively reducing bias; (B) the plots were collected at increasing voltages in the following order: V = 0, 0.05, 0.1, 0.15, 0.2, 0.25, 0.3 with arrow indicating the successively increasing bias; (C) the spectra indicates the contributions from two different time constants.

The characteristic patterns (high and low frequency arc) of the impedance spectra in the form of complex Nyquist plot for n^+-p junction solar cell are shown in Fig. 3. The Nyquist spectra in Fig. 3A, 3B and 3C shows the evaluation of A.C. response for silicon solar cell as the reverse, forward and back surface field (BSF) contributing bias across the terminal is varied, respectively.

In all the observed complex spectra, the symbols represent the experimental data points while the solid lines are fits to the model discussed in section 2. As the applied D.C. bias across the n^+-p junction is gradually decreased (i.e. reverse bias increases), the magnitude of complex impedance increases. This increase in the magnitude of complex impedance signifies the dielectric nature of n^+-p junction as the current flowing through the junction is very small or negligible. The capacitance and resistance of the n^+-p junction is dominated by the transition capacitance ($C_T = C_j$) and shunt resistance ($R_{sh} = R_j$) respectively. As the forward bias increases (0 to 0.4 V) across the terminal of n^+-p junction, radii of complex Nyquist plot reduces, signifying the conductive nature of n^+-p junction due to the increase in charge injection. The diffusion capacitance (C_d) and resistance (R_d) of n^+-p junction dominates at forward bias.

The contribution of p-p^+ junction is not detected in the impedance spectra until a strong forward bias is applied (> 0.5 V). This is due to the fact that at moderate forward bias, the voltage across n^+-p and p-p^+ junction acts to compress the space charge layer, consequently reducing the junction width. Also the p-p^+ junction is comparatively thinner than the n^+-p junction and base thickness, hence the net impedance at moderate forward bias is mostly influenced by the comparatively much larger impedance offered by the n^+-p junction. As the forward bias increases, an impedance arc at high frequency becomes gradually distorted due to the progressive involvement of resistive and capacitive components of p-p^+ as shown in Fig. 3C. Consequently the impedance contribution of p-p^+ region is added to achieve the satisfactory fits of the obtained data. At bias corresponding to knee voltage or at increased insolation, p-p^+ junction contributes to the high frequency part of complex Nyquist plot (Fig. 3C). Fig. 4 shows the voltage dependent variation of R_j for Silicon solar cell extracted from the low frequency arc of impedance spectra.

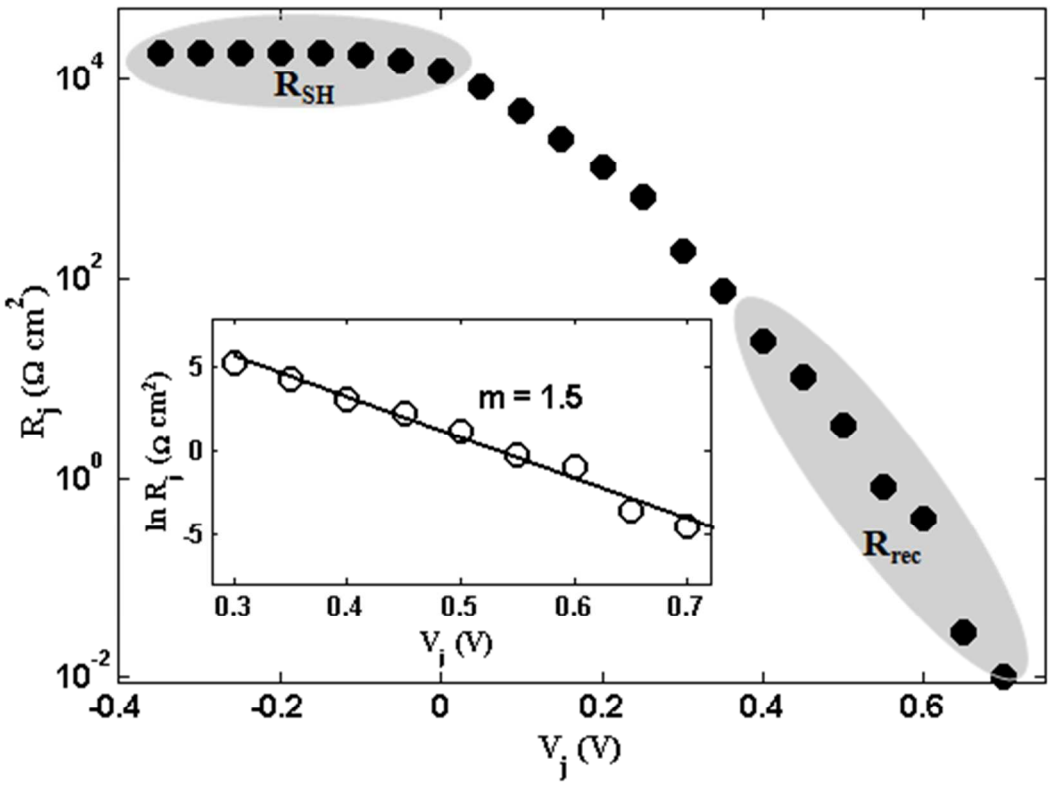

Fig. 4 Resistance of n^+-p junction measured using IS under different bias. The inset shows the plot of $ln\ R_j$ at a higher bias with the solid line indicating theoretical fit (Eq. (10) and Eq. (11) of ESI†).

Under reverse bias condition, the resistive component of Si solar cell is dominated by R_{SH} (as a consequence of unavoidable leakage current) and is nearly independent of junction voltage or illumination level. An insignificant voltage dependence of R_{SH} is observed in Fig. 4 which is consistent with the results reported by other groups [23-25]. At low forward bias, a change in the slope signifies a switching of predominant charge recombination process from SCR to the QNR. These recombination processes in SCR and QNR are often associated with two ideality factors, m_1 and m_2, having different values. In this article, an ideality factor (m_1) associated with the recombination mechanism in QNR region is of main interest due to the following reasons: (1) At

higher illumination level diffusion governed recombination is dominant, and (2) to account for the complex dynamic behavior of QNR with the increase in illumination level (junction voltage) as described below.

From the theory outline in section 2 and ESI†, it is indicated that with increasing illumination (or bias) electron density in the conduction band increases which results in a decrease of resistance offered by the junction (Eq. (10) and Eq. (11) of ESI†). Practically, an expected decreasing trend of R_j is observed (Fig. 4) for Si solar cell. With the increase in junction bias, R_j decreases by two to three order of magnitude as compared to R_{SH} at low illumination level. The obtained value of R_j at bias greater than knee voltage ($\approx 0.4\,V$ for 1 sun illumination) is mainly dominated by diffusion governed resistance R_d. The variation of R_j with bias infers about recombination flux by the following expression [24]:

$$R_j = \left(\frac{\partial I_{rec}}{\partial V}\right)^{-1} \qquad (5)$$

where I_{rec} is a recombination current and V is the applied junction voltage. The junction resistance (Fig. 4) follows an exponential behavior governed by $R_j = R_0 \exp\left(-\beta q V_F / k_B T\right)$. The theoretical curve fitting for R_j has been done with the following values: $R_0 = 1.8 \times 10^4\ \Omega$, $\beta = \frac{1}{m} \approx 0.67$ and $T = 298$ K. For an application of silicon solar cell at higher concentration (> 1 sun), a larger junction resistance R_j is desired because R_j represents an opposition of electrical loss caused by the recombination at junction.

Fig. 5 shows the variation of junction capacitance (C_j), measured from the low frequency arc of Nyquist spectra as a function of junction bias (illumination level $V_{oc} \simeq V_j$).

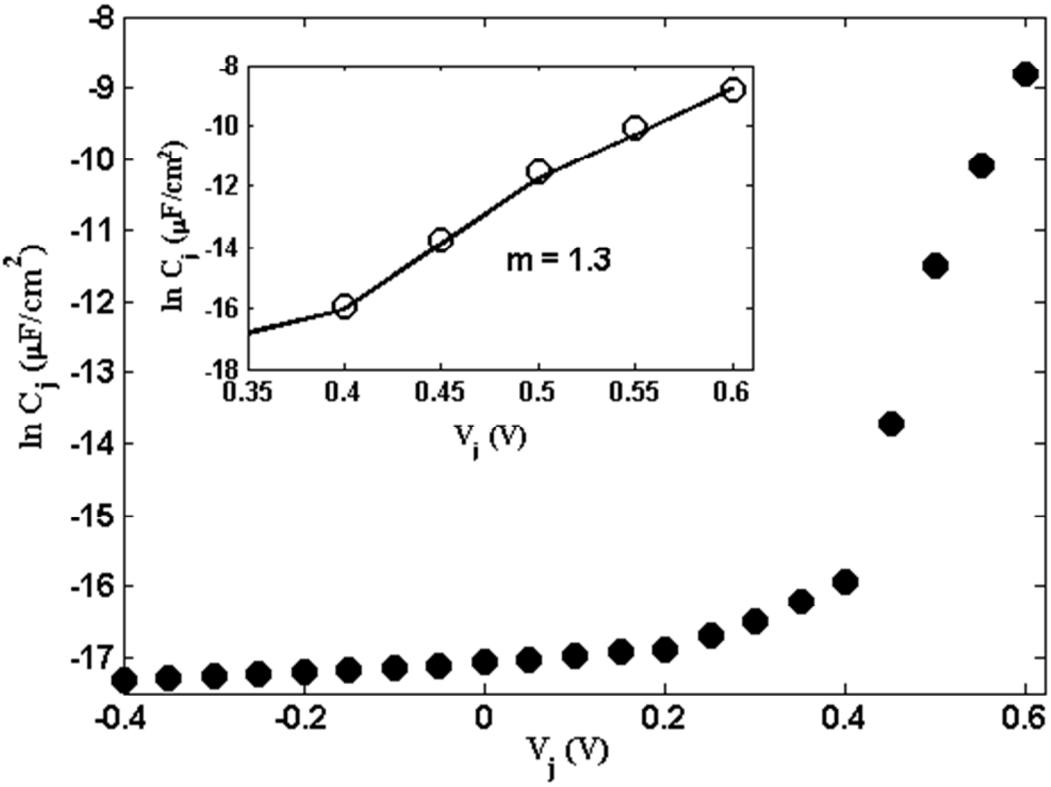

Fig. 5 Capacitance of n^+-p junction measured using IS at different bias. The inset shows the plot of $ln\ C_j$ at a higher bias with the solid line indicating theoretical fit.

The obtained variation of C_j is characterized in two different regions (Fig. 5) marked as low bias (≤ 1 sun) and a higher bias region (> 1 sun). A capacitance value at low bias (≤ 1 sun) is defined as the rate of change of total annihilated minority charge carriers in SCR by the applied junction bias i.e. (dQ/dV). An approximate expression for the capacitance is given as: $C_{dl} = C_{dl}^0 exp\left(V_j/m_2V_T\right)$ where $C_{dl}^0 = \left(|e|w_0n_i/4m_2V_T\right)$. The charge annihilated recombination of the generated electron and hole is dominated in the low bias region. The recombination gradually drops on both the sides of junction over the characteristic length w_0. A higher, almost constant and voltage independent value of C_j is observed in the low forward bias region indicating

dielectric behavior of Si material and a broader depletion region. The dielectric behavior is originated due to the following reasons: (1) due to the unoccupancy of density of state in silicon material, and (2) a depletion zone is built up at n^+-p junction which reduces to geometrical capacitance at zero bias voltage. At higher bias i.e. ($>V_{oc}$ at 1 sun), slightly different behavior of junction capacitance is observed for silicon solar cell than lower bias due to the following reasons: (1) exponential change in diffuse minority charge carriers, (2) occupation of the electronic density of states by excess minority charge carriers. The increase in illumination (or higher bias) results in an introduction of excess holes (Δp) with an insignificant change in the majority carriers (p_0) in the base region. Due to the change in majority charge carriers, the hole Fermi level shifts downward by $\Delta E_{F_p} = k_B T \ln p_0/(\Delta p + p_0)$, which is insignificant with respect to the shift in electron Fermi level (E_{F_n}). This indicates, E_{F_p} undergoes minor changes during photovoltaic operation [24]. Since the electron carrier density at equilibrium is negligible, the electron Fermi level E_{F_n} changes significantly when excess carriers are injected or photo generated at higher illumination level, which results in an exponential increase of the chemical capacitance. The capacitance plot also indicates a change in the slope as the applied bias increases from low FB to a higher FB. The obtained ideality factor from $R_d(V_j)$ fitting is nearly 15% larger than the ideality factor determined from fitting of $C_d(V_j)$ data. This suggests junction capacitance acts as a D.C. blocking element, and depends only on the junction width and doping density of the diffusion region. Therefore, the voltage dependent current carrying junction resistance is more sensitive to the presence of defects and recombination flux.

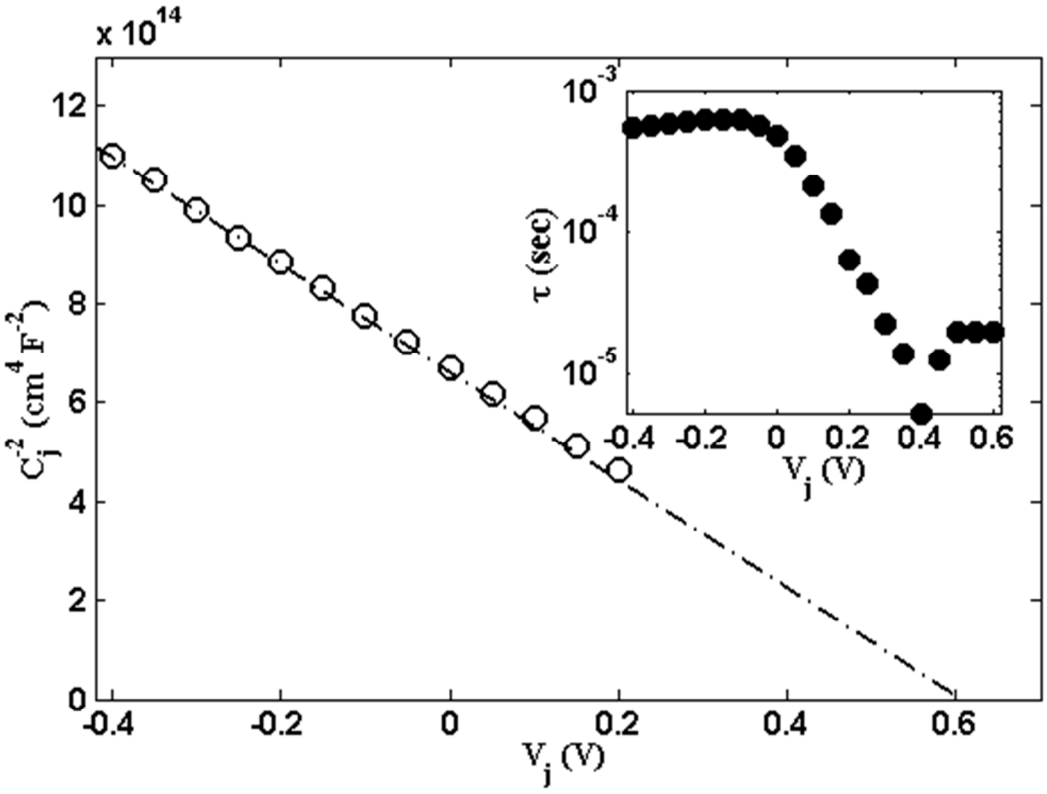

Fig. 6 Mott-Schottky plot of mono-crystalline Si solar cell. The inset shows the variation of minority carrier lifetime as a function of the applied bias.

The junction capacitance (transition capacitance) at reverse bias is represented by Mott-Schottky plot [32] in Fig. 6. The lines are the fit for the experimental data obtained using Eq. (16 of ESI†) indicating a linear fit to the composite data. The slope $\left({}^{2}/_{q\varepsilon N_a}\right)$, and the intercept, $\left({}^{2V_{bi}}/_{q\varepsilon N_a}\right)$ of the fitted line in Fig.6 provides the value of base doping concentration ($N_a \approx 1.5 - 4.0 \times 10^{16}\ \mathrm{cm}^{-3}$) and built-in potential ($V_{bi} \approx 0.6\,V$) and are comparable with the previously reported values [25, 28].

The inset of Fig. 6 shows the bias (illumination level) sensitive values of effective carrier lifetime (τ) obtained from Eq. (17 of ESI†). The trend of τ-V_j plot is different for low and high

forward bias regions, because under low bias conditions, recombination in SCR dominates while under high forward bias conditions, base recombination (QNR) dominates, which is in accordance with the theory outlined in ESI† and discussed previously with respect to Fig. 4 and Fig 5. At low forward bias, τ almost remains constant with respect to V_j by largely following the voltage independent behavior. This is mainly attributed to the following reasons: (1) due to the dielectric nature of silicon material, and (2) due to the increase in electric field in SCR with decreasing forward bias and thus widening the width at n^+-p junction. This eventually lowers the effective diffusion coefficients of charge carriers in the active region of the fields. At higher forward bias, τ follows the voltage dependence of R_j, which arises from the injection dependent carrier lifetime. The dependence of τ at bias corresponding to maximum power point reflects the competitive interplay between two types of recombination mechanism associated with SCR and QNR. Hence the net recombination process is most efficient in this region (i.e., 0.35-0.45 V). The effective lifetime in base region is lower in the voltage range where the efficient charge annihilation occurs. In view of Fig. 1, it is most likely that the general trend is affected by both, SCR as well as QNR recombination.

4.2. Current-voltage characteristics

Fig. 7 shows the voltage dependent photocurrent (I_{PH}) of silicon solar cell at 25℃ for varied illumination level from 1 to 12.2 suns.

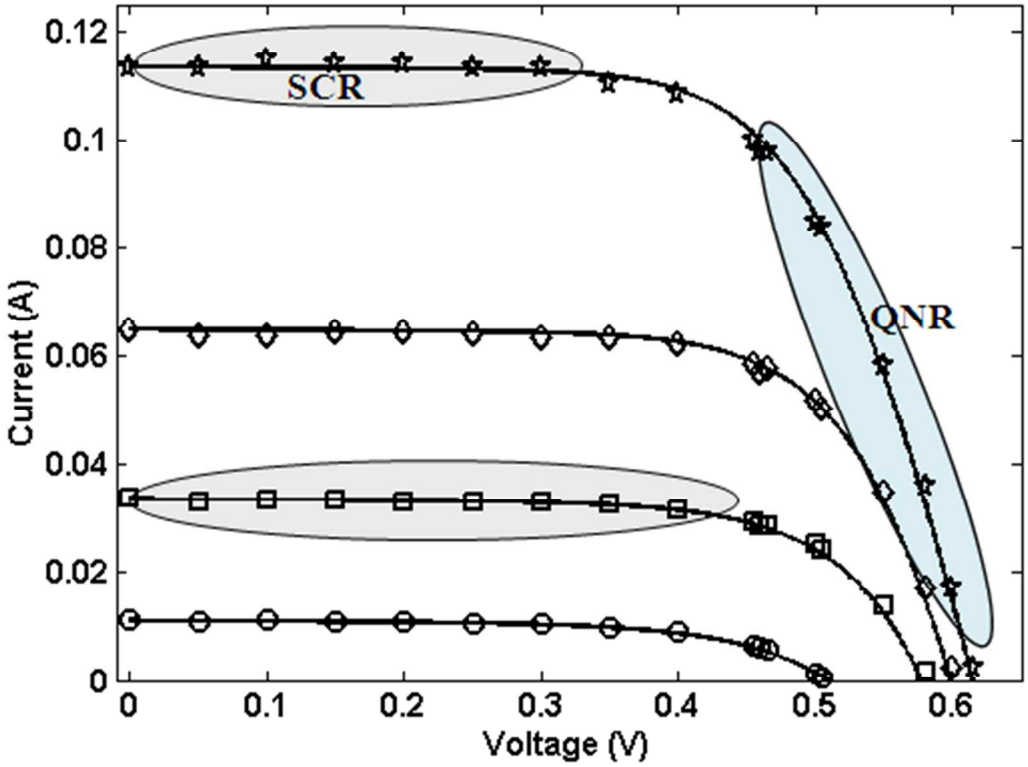

Fig. 7 Current-voltage characteristics of mono-crystalline Si solar cell with varying illumination levels (1 sun corresponds to AM1.5, 1000 W/m^2) (circle: ~1 sun, square: ~ 3 suns, diamond: ~6 suns and star: ~10 suns). The marked region shows the QNR and SCR governed recombination regions.

In Fig. 7, the solid line represents the theoretically fitted data from the proposed model given in section 2 and the points represent the experimental data. An excellent agreement with $\leq \pm 5$ % error between experimental data and theoretical calculation is obtained. The static parameters I_{SC}, V_{OC}, P_{max}, FF, η and R_s of Si cell measured under STC conditions and calculated from the proposed model (section 2) are summarized in Table 1. An increase in current (I_{SC}) and open circuit voltage (V_{OC}) with the change in illumination level at constant temperature is observed. Under non equilibrium conditions, promotion of electron in acceptor state and hole to

donor state results in shifting of electron Fermi level E_{F_n} towards higher side (in terms of energy) while the hole Fermi level E_{F_p} undergoes a small downward shift, the difference of these energy values is often associated with the V_{OC} of solar cell as given by Eq. 6 (ESI†). For Si solar cell studied here under irradiation (λ) with generation rate (G) and AM1.5 spectrum (with concentration ratio (CR) from >1-12 suns), an increase in illumination causes E_{F_n} and E_{F_p} to shift towards higher and lower energy level respectively resulting in an increase of V_{OC} (Fig. 7). This observation is further supported by the C-V plot (Fig. 5) where the electron occupation in density of states increases with an increase in forward bias corresponding to illumination dependent V_{OC}. The similar trend for V_{OC} has been obtained by other researchers [33]. A linear increase in I_{SC} with illumination level signifies an increase in generation of electron hole pairs and occupancy of density of state till quasi flat band condition is achieved.

From the obtained I-V characteristics (Fig. 7), recombination in QNR is dominant over SCR resulting in a shift of maximum power point (MPP) towards the lower voltage. The extracted parameters from I-V plot (Fig. 7) describe the dependence of η and *FF* on illumination level for a Si solar cell. From the obtained parameters listed in Table 1 (R_S and m used as fitting parameters), it can be observed that η and *FF* increase to a maximum of 16.8% and 69% respectively at illumination level of ≈5.8 suns and then decreases linearly with an increase in illumination level. The dynamic trend of η and *FF* with the change in illumination level mainly depends on the competitive interplay between V_{OC}, R_S and m of a solar cell. Under low illumination or optimum CR level, a logarithmic dependence of V_{OC} $\left(V_{OC}(CR) = {kT}/{q}\, ln\left({I_{sc} \times CR}/{I_0} + 1\right)\right)$ on the concentration ratio (CR) and I_{SC}, causes an

increase in FF and η of Si solar cell (Table 1). Whereas, beyond the optimum CR level (where the influence of V_{OC} is minimized), a mixed activation of R_S and m causes a reduction in η and FF. The series resistance of solar cell is governed by the front contact grid of silver, back contact layer of aluminum and carrier transporting interlayer (n^+-p, p active layer and p-p^+) having a functional dependence on illumination, temperature and generation and recombination of charge carriers [25]. With an increase in illumination level beyond optimum CR a higher charge transport within the interlayer of silicon material, finger and bus bar causes higher resistive power loss equivalent to I^2R_S in the solar cell thus reducing its η and FF. A similar trend of series resistance with illumination and temperature for mono-crystalline silicon solar cell is observed by Garland et al. and Khan et al. [25, 34]. The dominance of QNR over SCR diffusion recombination is another factor for lowering the η and FF of Si solar cell beyond an optimum CR. According to Shockley-Read-Hall recombination effect, an ideality factor (m) of 2 signifies that the recombination takes place via a single trap level in SCR [27]. This process is observed to a measurable extent only at low forward bias conditions where the QNR recombination is practically absent. On the other hand, an ideality factor (m) of 1 at high forward bias signifies diffusion of charge carriers in QNR where the effect of SCR recombination is almost negligible [27]. From Fig.7 and extracted parameters in Table 1, the diode ideality factor m is equal to 2.5 (average value at scan voltage range between 0 to 0.4 V) under 1 sun illumination, mainly dominated by SCR recombination. With an increase in illumination level, the ideality factor reduces to ~1.5 and attributed to the dominance of QNR governed recombination. Similar behavior for ideality factor (m) with illumination is observed by other researchers [27, 33, 34]. From the abovementioned discussion, it can be concluded that a logarithmic dependence of V_{OC}

on CR causes an increase in η and *FF*, whereas a linear decrease of *m* along with the linear increase in R_S causes a reduction in η and *FF*.

Table 1: Performance indicating parameters extracted from Fig. 7 for mono-crystalline silicon solar cell (active area: 0.34 cm^2)

Parameters		I_{SC} (mA)	V_{OC} (V)	FF (%)	P_{MAX} (mW)	η (%)	R_s (Ω)	*m*
1 sun	Theory	11	0.509	62.1	3.5	12.9	0.02	2.5
	Experiment	11.1	0.507	64.5	3.6	13.2	-	
3.034	Theory	33.67	0.574	68.5	13.2	15.9	0.02	2.3
	Experiment	33.68	0.578	68.7	13.4	16.2	-	
5.852	Theory	64.92	0.598	69.1	26.8	16.8	0.4	1.9
	Experiment	64.96	0.600	68.9	26.8	16.8	-	
10.227	Theory	113.4	0.614	66.0	46.0	16.5	0.6	1.7
	Experiment	113.5	0.615	65.2	45.5	16.3	-	
12.2	Theory	135.5	0.609	62.0	51.4	15.4	0.8	1.5
	Experiment	135.4	0.608	62.3	51.0	15.3	-	

5. CONCLUSIONS

A detailed theoretical platform is presented to explain the results of D.C. and A.C. characteristics of mono-crystalline Si solar cell subject to low-concentration illumination conditions. Contributions of different solar cell parameters, diffusion capacitance, transition capacitance,

diffusion resistance, recombination resistance and back surface field has been resolved using A.C. impedance spectroscopy technique. The feasibility of commercially available mono-crystalline Si solar cell for LCPV applications has been explored by D.C. current-voltage characteristics under varying illumination. The finding reported here demonstrates the importance of D.C. and A.C. characterization for evaluation of performance indicating parameters of Si solar cell under non-equilibrium conditions differing from 1 sun.

ACKNOWLEDGEMENTS

The authors acknowledge the financial support provided by Gujarat Energy Development Agency (GEDA) to develop CPV system by grant number: GEDA\EC:REC\March-2010/3/9174. The authors also acknowledge Neety Euro-Asia Solar Energy, India for providing technical help for this study. The authors acknowledge Prof. Indrajit Mukhopadhyay and Dr. Abhijit Ray for scientific discussions.

†Electronic Supplementary Information (ESI) available.

REFERENCES

1. P. Yadav, B. Tripathi, M. Lokhande and M. Kumar, *Sol. Energy Mater. Sol. Cells*, 2013, 112, 65–72.
2. V. A. Chaudhari and C. S. Solanki, *International Journal of Photoenergy*, 2009, http://dx.doi.org/10.1155/2009/827402.

3. C. S. Solanki, *Solar Photovoltaics: Fundamental, technologies and applications,* Prentice Hall, India, 2nd edition, 2011.
4. I. A. Schwirtlich, in *High-Efficient Low-Cost Photovoltaics*, Springer Series in Optical Sciences, Springer, Berlin, Germany, 2009, 140, pp. 57–64.
5. B. Pivac, V. Borjanovi, I. Kovacevi, B. N. Evtody and E. A. Katz, *Solar Energy Materials and Solar Cells*, 2002, 72, 165–171.
6. P. A. Basore, *Proceedings of the 4th IEEE World Conference on Photovoltaic Energy Conversion (WCPEC'07)*, 2007, 2, 2089–2093.
7. A. Cuevas, R. A. Sinton, N. E. Midkiff and R. M. Swanson, *Electron Device Letters*, 1990, 11, 6–8.
8. B. Tripathi, P. Yadav, M. Lokhande and M. Kumar, *International Journal of Electrical and Electronics Engineering Research*, 2012, 2, 84-93.
9. S. Kurtz, *Opportunities and challenges for development of a mature concentrating photovoltaic power industry*, Technical Report, NREL/TP-520- 43208, 2009.
10. Cogenra, http://www.cogenra.com/product/product-overview (accessed on 20-01-2014).
11. M. Castro, I. Anton and G. Sala, *Sol. Energy Mater. Sol. Cells*, 2008, 92, 1697-1705.
12. M. Li, X. Ji, G. Li, S. Wei, Y. Li and F. Shi, *Applied Energy*, 2011, 88, 3218-3227.
13. A. Zahedi, *Renewable and Sustainable Energy Reviews*, 2011, 15, 1609–1614.
14. M. A. Schuetz, K. A. Shell, S. A. Brown, G. S. Reinbolt, R. H. French and R. J. Davis, *IEEE Journal of Photovoltaics*, 2012, DOI 10.1109/JPHOTOV.2012.2186283.
15. F. Reis, M. C. Brito, V. Corregidor, J. Wemans and G. Sorasio, *Sol. Energy Mater. Sol. Cells*, 2010, 94 1222-1226.
16. Solaria, http://www.solaria.com/products/technology.html (accessed on 20-01-2014).

17. Akhter Solar, http://www.akhtersolar.com/Documents/Concentrated%20PV%20Modules/JN-1476-Si-Con-4x-low-concentration-PV-15-05-09.pdf (accessed on 19-01-2014).
18. Everphoton, http://www.everphoton.com/elcpvproduct.html (accessed on 19-01-2014).
19. Amonix, http://amonix.com/pressreleases/amonix-achieves-world-record-359-module-efficiency-rating-nrel-4 (accessed on 18-01-2014).
20. P. Yadav, B. Tripathi and M. Kumar, *International Journal of Photoenergy*, 2013, http://dx.doi.org/10.1155/2013/929235.
21. P. Yadav, B. Tripathi, M. Lokhande and M. Kumar, *AIP Journal of Renewable and Sustainable Energy*, 2013, 5, 013113-1-10.
22. P. Yadav, B. Tripathi, S. Rathod and M. Kumar, *Renewable & Sustainable Energy Reviews*, 2013, 28, 812-823.
23. J. E. Garland, D. J. Crain, J. P. Zheng, C. M. Sulyma and D. Roy, *Energy Environ. Sci.*, 2011, 4, 485-498.
24. I. Mora-Sero, G. Garcia-Belmonte, P. P. Boix, M. A. Vazquez and J. Bisquert, *Energy Environ. Sci.*, 2009, 2, 678-686.
25. J. E. Garland, D. J. Crain and D. Roy, *Sol. Energy*, 2011, 85, 2912-2923.
26. R. A. Kumar, M. S. Suresh and J. Nagaraju, *IEEE Trans. Power Electron.*, 2006, 21, 543-548.
27. D. J. Crain, S. E. Rock, J. E. Garland and D. Roy, *Curr. Appl. Phys.*, 2013, 13, 2087-2097.
28. D. J. Crain, J. E. Garland, S. E. Rock and D. Roy, *Anal. Methods*, 2012, 4, 106-117.

29. M. Veerachary, T. Senjyu and K. Uezato, *IEEE Transactions on Aerospace and Electronic Systems* 2002, 38, 262-270.

30. M. Veerachary and K. S. Shinoy, *IEE Proceedings-Electric Power Applications*, 2005, 152, 1263-1270.

31. H. L. Tsai, C. S. Tu and Y. J. Su, *Proceedings of the World Congress on Engineering and Computer Science*, October 22 - 24, San Francisco, USA, 2008.

32. S. M. Sze, Physics of semiconductor devices, Wiley, New York, 2nd ed., 1981.

33. B. Gupta, P. K. Shishodia, A. Kapoor, R. M. Mehra, T. Soga, T. Jimbo and M. Umeno, *Sol. Energy Mater. Sol. Cells*, 2002, 73, 261-267.

34. F. Khan, S.N. Singh and M. Husain, *Sol. Energy Mater. Sol. Cells* 2010, 94, 1473-1476.